Image Anal Stereol 2026;45:75-94 doi: 105566/ias.3953
Original Research Paper

3D IMAGING AND QUANTITATIVE ANALYSIS OF DIGESTIVE GLANDS MORPHOGENESIS IN CRUSTACEAN DEVELOPMENT: APPLICATION OF MICRO-CT, LIGHT AND ELECTRON MICROSCOPY

POLONA MRAK[1,✉], URBAN BOGATAJ[1], KATJA KUNČIČ[1], MILOŠ VITTORI[1] AND NADA ŽNIDARŠIČ[1]
[1]Department of Biology, Biotechnical faculty, University of Ljubljana, Slovenia.
e-mail: polona.mrak@bf.uni-lj.si, urban.bogataj@bf.uni-lj.si, katja.kuncic@bf.uni-lj.si, milos.vittori@bf.uni-lj.si, nada.znidarsic@bf.uni-lj.si.
(Received March 16, 2026; revised April 3, 2026; accepted April 4, 2026)

ABSTRACT

The processes of morphogenesis during animal development are complex and interdependent at all organisational levels. Thus, it is beneficial to visualize morphogenesis at different scales and including 3D imaging and quantification. Here the application of a combination of complementary imaging techniques (micro-computed tomography, histology, and transmission electron microscopy), supplemented by morphometrical analyses, is presented in a study of digestive glands morphogenesis during embryonic and postembryonic development of isopod crustacean. The first pair of gland tubules is formed in mid-stage embryo from gland primordium, separated into two lobes by gland epithelium longitudinally from posterior to anterior direction. The width reduction and volume decrease of the tubules were observed from late embryo through marsupial and postmarsupial mancae stages. The second pair of gland tubules starts to form in mid-stage embryo S14 and elongates from late embryo onwards, with gradual volume increase. Epithelial cells of digestive glands are morphologically modified from cuboidal to the dome-shaped B cells and wedge-shape S cells in late marsupial mancae, which coincides with complete depletion of yolk within gland lumen. Septate junctions in gland epithelium elongate from embryos to postmarsupial mancae, while their ultrastructure does not change considerably. The most intense elongation of septate junction was evident at transition from marsupial to postmarsupial manca stage, which is consistent with release of the animal from marsupium to the external environment. Integration of data acquired by the presented imaging techniques and quantitative analyses allowed us to relate histological and ultrastructural modifications of epithelium to crucial transitions in digestive gland morphogenesis and to the key steps of animal embryonic and postembryonic development.

Keywords: 3D anatomy, embryonic and postembryonic stages, morphometry, septate junction.

INTRODUCTION

Imaging of biological samples at different scales is crucial to obtain an integrative view on distinctive morphology and functions from molecular to organ level in the context of the whole organism (Handschuh *et al.*, 2013; Walter *et al.*, 2020; Rudraiah *et al.*, 2024). The structures and processes within a living organism are complex and interdependent throughout all levels of biological organisation, thus it is beneficial to visualize structures by 3D imaging and across multiple scales, supplemented by quantitative analysis of the relevant morphological parameters. Integration of data from multiple imaging approaches allows us to gain much more complete information on the morphogenetic process that are beyond the information gained from one individual technique used. In addition, studies of developmental processes demand the analysis of sequential developmental stages, thus it is necessary that stages are well defined temporally and morphologically for the species investigated.

Morphogenetic processes involved in organism development are deeply conserved within the animal kingdom. The advancement of understanding the tissue and organ morphogenesis and the application of these concepts in various fields of bioscience are achieved through the multidisciplinary investigations of animal embryonic and postembryonic development. Imaging of embryos and larvae by complementary methods is one of the key tools, which allows us to study the developmental processes in the physiological environment and from individual cells to the whole organism. A comprehensive survey of methods applied to study organogenesis in decapod crustacean larvae, focused to classical and state-of-the-art imaging techniques, is presented by

Torres *et al.* (2021) and Melzer *et al.* (2021). To advance knowledge on digestive glands morphogenesis and on different aspects of the organ functional specialisations during development, morphogenesis of digestive glands tubules and their epithelium as an integrative part of organogenesis needs to be elucidated, as this process is crucial for shaping of organs and for establishment of organs' vital functions. The digestive gland epithelium functions as transporting epithelium, a selectively permeable barrier in organ, in which complex regulation of paracellular fluxes depends on occluding junctions, in invertebrates the septate junctions (Jonusaite *et al.*, 2016).

In crustaceans, the digestive glands, also named midgut glands or hepatopancreas, are a part of the digestive system with numerous essential functions in nutrients processing. Together with midgut, the digestive glands are the endodermal parts of crustacean digestive system. They consist of several blindly ending tubules, even hundreds in decapods, which are connected to the digestive tract. The tubules are composed of single-layered epithelium, which in decapods includes five specialized cell types, E cells (embryonic cells), R cells (resorptive cells), F cells (fibrillar cells), B cells (blister-like cells) and M cells (midget cells) (Štrus *et al.*, 2019; Vogt, 2019). In isopod crustaceans, the endodermal parts are reduced and in terrestrial isopods the midgut region within digestive tract is absent (Hames and Hopkin, 1989; Storch and Štrus, 1989; Wägele, 1992). Digestive glands are composed of paired blind-ending tubules, which open into the digestive tract at the junction of the foregut and hindgut (Štrus *et al.*, 1995) and perform a broad range of functions, i.e. absorption, storage of lipids, carbohydrates, proteins and metals, secretion, excretion and probably osmoregulation (Storch, 1984). A short midgut region situated in-between the foregut and hindgut, and connected to the digestive glands, was described in amphibious species of the family Ligiidae (Štrus and Drašlar, 1988; Štrus *et al.*, 1995). The digestive glands in adult animals of isopod *Porcellio scaber* consist of four spiral tubules, formed by epithelium composed of hepatopancreatic B and S cells. Each tubule is surrounded by the neuromuscular network. Dome shaped B or large cells alternate with wedge shaped S or small cells (Storch, 1984; Bettica *et al.*, 1984; Wägele, 1992; Žnidaršič *et al.*, 2003).

Digestive glands in decapods emerge from midgut canal near the connection with the stomach during early larval development, in the shape of paired lobes. The initial lobes already include the same cell types as in adults and R cells are observed to have an important function in lipid storage. Later during larval development, the lobes ramify into numerous tubules of smaller diameter, which elongate (Lowett and Felder, 1989; Biesiot and McDowell, 1995; Abrunhosa and Kittaka, 1997; Diaz *et al.*, 2008; Vogt, 2008; Tziouveli *et al.*, 2011; Muhammad *et al.*, 2012; Spitzner *et al.*, 2018; Štrus *et al.*, 2019; Kalacheva *et al.*, 2023). In Peracarida, individual aspects of the digestive glands' morphogenesis were partly described only in amphipod *Parhyale hawaiensis* (Browne *et al.*, 2005), in parasitic isopod *Paragnathia formica* (Manship *et al.*, 2011) and in terrestrial isopod *Porcellio scaber* (Štrus *et al.*, 2008; Wolff, 2009; Milatovič *et al.*, 2010). These studies aimed to establish the staging system for the investigated species; thus, they were focused mainly on the morphological characteristics important for identification of the developmental stages and not on characterization of the digestive glands morphogenesis in detail. In all three species the digestive glands become significant already during embryonic development, involved in the degradation and absorption of yolk. The yolk within glands is consumed till release from the female marsupium, when animals become dependent on external food sources (Štrus *et al.*, 2019). One of the crucial differentiation processes that enable adequate barrier and transport functions of invertebrate epithelium in general is the formation of septate junctions, which has not been characterized during digestive glands morphogenesis previously. Septate junctions in invertebrate epithelia play also a role in tissue morphogenesis, as studied e.g. during the formation of tracheae, salivary glands, midgut and Malpighian tubules (Rouka *et al.*, 2021). Septate junctions are characterized by electron dense septa in the intercellular space (Izumi and Furuse, 2014; Jonusaite *et al.*, 2016), which can vary in number or distribution depending on the function of the epithelium (Jonusaite *et al.*, 2016). A continuous array of septa located subapically forms smooth septate junction in the epithelium of the digestive glands. Above all, in crustaceans there are several studies, which include at least two imaging techniques to investigate digestive system in developmental stages, and mostly combine histology with micro-CT or electron microscopy, but they are limited to decapod larval stages (Vogt, 2008; Tziouveli *et al.*, 2011; Castejon *et al.*, 2018; Spitzner *et al.*, 2018; Castejon *et al.*, 2021; Sonakowska-Czajka *et al.*, 2021; Kalacheva *et al.*, 2023). A detailed structure of digestive glands during morphogenesis, comprising 3D imaging, quantification of selected morphological parameters and detailed histological and ultrastructural analyses of digestive glands epithelium during embryonic and postembryonic, was not studied before in crustaceans, and very rarely even in other species. The isopod species *P. scaber*, with a well-established developmental staging system, enables

us to obtain *"in situ*" insight into organ morphogenesis from a broader perspective of organism development, tissue formation and cell differentiation.

In this study, we aim (i) to introduce a combination of complementary imaging techniques to study organ morphogenesis across multiple scales, including 3D imaging and quantitative analysis, and integrate the data into a broader view; and (ii) to characterize digestive glands morphogenesis during *P. scaber* embryonic and postembryonic development, with a focus on the morphogenesis of the first and the second pair of gland tubules, and on differentiation of epithelial cells and septate junctions. We have comprehensively characterized the digestive glands in the selected sequential developmental stages with the integration of following imaging techniques: micro-computed tomography (micro-CT), histology and transmission electron microscopy (TEM), supplemented with the morphometry of the selected glands' features. Our study addresses specifically modifications of the shape and volume of the digestive gland tubules, transformation of the epithelial cells' shapes and alterations of length and ultrastructural architecture of septate junctions in the gland epithelium. We expect that major changes of digestive glands shape and volume coincide with the key modifications of epithelial cell shape and septate junctions differentiation during morphogenesis in embryonic and postembryonic development.

MATERIAL AND METHODS

REARING OF ANIMALS AND COLLECTION OF EMBRYOS AND MANCAE

Specimens of isopod crustacean *P. scaber* (Latreille, 1804) were reared in a glass terrarium at 22-25 °C, high humidity and a 12h light/dark cycle. Embryos and marsupial mancae were isolated from the marsupia of gravid females, and their developmental stages were determined, using the staging system of Milatovič *et al.* (2010) and Mrak *et al.* (2012). The following developmental stages were analysed in this study: three stages of mid-stage embryos (S13, S14 and S15), late embryos (S16), early-, mid- and late-stage marsupial mancae and postmarsupial mancae. Postmarsupial mancae were collected at two time points after release from marsupium: (i) 1-3 days after release for all analyses applied; (ii) 14 days after release for additional histology and ultrastructure analyses. For micro-CT analysis, the anaesthetized adult specimens were perforated by a thin needle on the ventral body surface and their pereopods were removed, which improves the impregnation of the sample with chemical solutions during further procedure. For histological and ultrastructural analyses of the digestive glands in adults, the glands were isolated from anaesthetized adult animals that showed no signs of moulting.

MICRO-CT: SAMPLE PREPARATION, ACQUISITION OF X-RAY PROJECTION IMAGES, RECONSTRUCTION AND POST-PROCESSING OF THE VIRTUAL 3D DATA SET

Immediately after isolation, fixation of samples was performed in 2% formaldehyde (FA) and 2.5% glutaraldehyde (GA) in 0.1 M HEPES buffer. After fixation, the samples were rinsed with HEPES buffer. To evaluate the effect of sample osmification, some samples of the embryonic and post-embryonic stages were post-fixed with 1% osmium tetroxide (OsO_4) for 2 hours, while other samples were kept non-osmicated. All samples were gradually dehydrated in increasing concentrations of ethanol as follows: 50% ethanol, 70% ethanol, 80% ethanol, 90% ethanol, 96% ethanol, 100% ethanol. We then replaced the ethanol with hexamethyldisilazane (HMDS), and after the two HMDS incubations, each for 30 minutes, we discarded the HMDS and left the samples overnight in a fume hood to allow the HMDS to evaporate completely. The specimens were attached to pipette tips with superglue (adult specimens) or carbon adhesive tape (embryos and mancae), which allowed easy placement on the holder in the microtomograph.

We analysed the samples using an N80 microtomograph (Neoscan) equipped with Neoscan80 software. During imaging, we rotated the sample by at least 180° with a rotation step of 0.2°. After acquisition, a set of recorded projection x-ray images was imported into the Neoscan80 program, and a 3D stack of sequential 2D cross-sections of the sample in the z-axis was reconstructed by a filtered back projection algorithm. These 3D stacks were imported into Dragonfly software (Comet) for 3D reconstruction and organ segmentation (Fig. 1). Segmentation of digestive glands was performed by manual labelling.

QUANTIFICATION OF DIGESTIVE GLANDS AND YOLK VOLUME

The micro-CT method allowed us to perform quantification of the digestive glands volume, represented by gland epithelium and lumen, and quantification of the yolk volume outside the digestive glands in different developmental stages, using the 3D reconstructions. The volume of yolk and digestive glands were

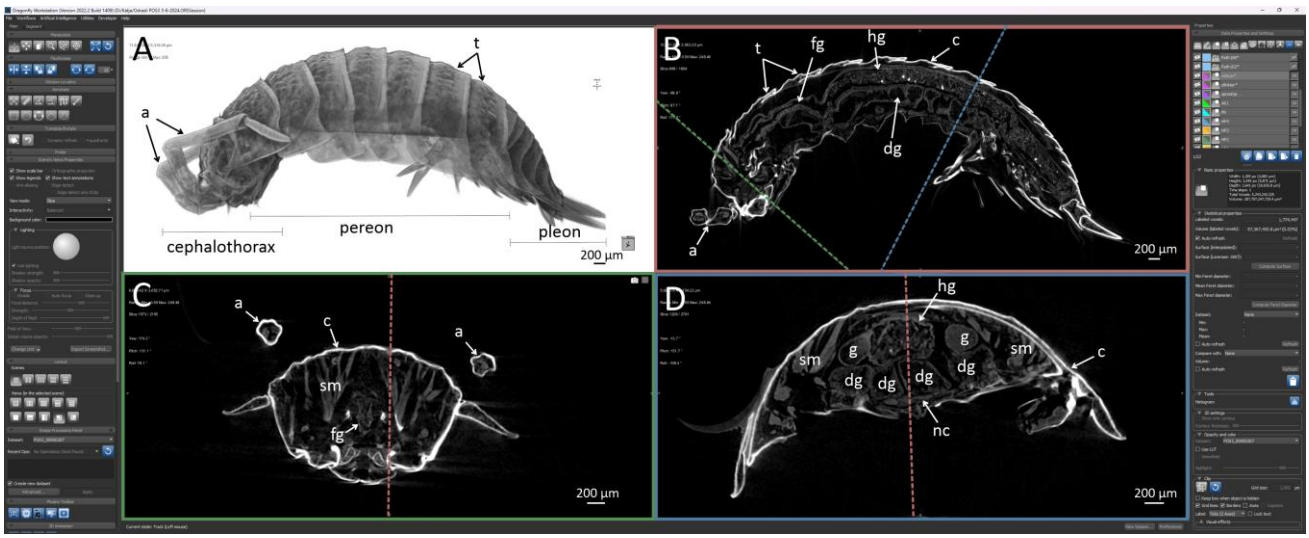

Fig. 1. *Analysis of micro-CT images of P. scaber adult by Dragonfly software. Based on the images, manual segmentation of the digestive glands was performed. The image shows the four-panel display mode: A) 3D reconstruction of the whole animal, showing 3 body regions, cephalothorax, pereon and pleon. Pereopods were removed before sample fixation. B) A virtual 2D sagittal section of an animal is shown (red frame). The green and blue dotted lines show the axes and locations of the virtual cross sections shown on panels (C) and (D). C and D) A virtual 2D cross section of the animal in the anterior region (C, green frame) and in the posterior region (D, blue frame). The red line shows the axis and location of the virtual 2D section on panel (B). a – antennae, g – gonads, c – exoskeletal cuticle, sm – skeletal muscles, fg – foregut, hg – hindgut, dg – digestive glands, t – tergites, nc – ventral nerve cord.*

quantified based on the number of marked volume elements (voxels). The volumes were measured on three specimens per each analysed stage: S13 embryos, S14 embryos, S16 embryos, early- mid- and late marsupial mancae and postmarsupial mancae, altogether 21 samples. Data are presented graphically with individual data spots in the separate diagrams for the first and the second pair of the digestive gland tubules in each presented developmental stage. Additionally, the mean values (with standard error bars) of the volumes for each developmental stage are presented in the common diagram by columns, with the volumes of the external yolk, the first and the second pair of glands presented by different colours. The graphs were prepared in GraphPad Prism software.

HISTOLOGY AND TRANSMISSION ELECTRON MICROSCOPY

Fixation was performed in 2.5% GA in 0.1 M cacodylate buffer for the samples of embryos and mancae and in 3.5% GA in 0.1 M phosphate buffer for isolated glands from adults. After transferring the embryos to the fixative, the embryonic envelopes were carefully perforated by a thin needle. After fixation, all samples were rinsed with the same buffer that was used in the fixative, and then post-fixed for 1-2 hours with 1% OsO_4. After rinsing in Milli-Q water, the samples were dehydrated in increasing concentrations of ethanol as follows: 50% ethanol, 70% ethanol, 80% ethanol, 90% ethanol and 100% ethanol. The samples were transferred to 100% acetone and then gradually embedded in resin. The samples of digestive glands of adults were embedded in Spurr resin, embryos and mancae were embedded in Agar 100 resin. The exoskeletal cuticle of mancae was perforated by a thin needle before the embedding for better resin infiltration. Resin was polymerized for at least 24 hours at 60°C (Agar 100) or at 70°C (Spurr).

Sections of the samples embedded in resin were prepared using a Reichert Ultracut S (Leica) ultramicrotome or an EM UC6 (Leica) ultramicrotome. For light microscopy, semithin sections of 0.5 µm thickness were prepared and stained with Azure II – methylene blue dye (Richardson staining). They were examined and documented with an AxioScope Opton light microscope (Zeiss) equipped with a Leica DFC290HD digital camera and LAS V4.0 software, or with an AxioImager Z.1 light microscope (Zeiss) equipped with an HRc digital camera and AxioVision 4.5 software (Zeiss).

For transmission electron microscopy, ultrathin sections of 70 nm thickness were prepared using a Diatome ultra 45° diamond knife, contrasted and imaged with a CM 100 transmission electron microscope (Philips) equipped with an SC 200 Orius digital camera (Gatan) and Digital Micrograph software (Gatan).

QUANTIFICATION OF THE SELECTED ULTRASTRUCTURAL CHARACTERISTICS OF SEPTATE JUNCTIONS

We measured selected characteristics of the septate junctions using Fiji/ImageJ software (version 2.14.0/1.54f) for analysing microscopic images. The following measurements were performed: (i) length of the septate junction (lSJ) - the length of the junction from the first to the last septa, following the course of the septa series along cell membranes; (ii) length of the septate junction straight line (slSJ) - the shortest distance between the first and the last septa; (iii) the width of the intercellular space in the region of septate junction; (iv) the distance between consecutive septa in the septa array; (v) the thickness of individual septa (Fig. 2). All measurements were performed in the Fiji/ImageJ program using the tools "Segmented Line" or "Straight Line". Linearity index of the septate junction was calculated as lSJ/slSJ (INSJ), based on the studies Otani *et al.* (2006) and Brezovjakova *et al.* (2019), and provides information of the extent of membrane folding in the junction area. The closer the value is to 1, the more straight the junction is, while higher index values indicate greater folding of the junction.

Measurements of septate junctions' length were applied in 10 specimens of different developmental stages and adults, with the following number of junctions measured: 17 junctions in 3 embryo specimens (S13 and S16); 26 junctions in 3 marsupial manca specimens; 15 junctions in one postmarsupial manca 14 days after release; 30 junctions in 3 adult specimens. The measurements of the width of the intercellular space were applied in 9 specimens and in the following number of junctions: 47 junctions in 3 embryo specimens (S13 and S16); 59 junctions in 3 marsupial manca specimens; 103 junctions in 3 adult specimens. The septa distance was measured in 6 specimens, with the following number of junctions measured: 10 junctions in 2 embryo specimens (S13 and S16); 7 junctions in 2 marsupial manca specimens; 40 junctions in 2 adult specimens. The septa thickness was measured in 6 specimens, with the following junctions measured: 12 junctions in 2 embryo specimens (S13 and S16); 11 junctions in 2 marsupial manca specimens; 50 junctions in 2 adult specimens. Results are presented graphically with box plots, prepared in GraphPad Prism software. Box plots depict the minimum, 1st quartile, median, 3rd quartile and maximum and all individual data points are presented.

RESULTS

MORPHOGENESIS OF THE FIRST AND THE SECOND PAIR OF DIGESTIVE GLAND TUBULES IN THE MID-STAGE AND LATE EMBRYOS

Morphogenesis of digestive glands in mid- and late-stage embryos was characterized in the context of the whole embryo on virtual 2D sections and 3D reconstructions recorded by micro-CT (Figs. 3, 4, 5). The morphology of the organs and tissues in embryos, which are only about 0.8 mm in size, were recognized by micro-CT. The digestive gland primordium in mid- and late-stage embryos occupies a great majority of the embryo volume, incorporating yolk into its lumen (Fig. 3, 4). External and internal anatomy of the embryo was clearly resolved by micro-CT, including head with stomodeum anteriorly, body segments, pereopod primordia ventrally and proctodeum dorso-posteriorly (Figs. 3, 4, 5).

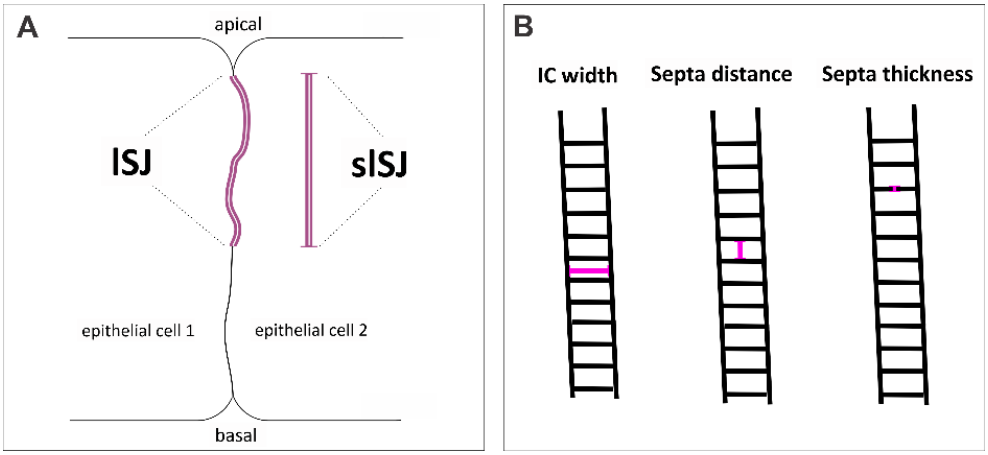

Fig. 2. *Schematic representation of the characteristics of septate junctions in digestive gland epithelium quantified in the study. (A) lSJ - the length of septate junction following the course of the membranes; slSJ - the straight-line length of septate junction, defining the shortest distance between endpoints of the junction. The linearity index INSJ is a value calculated as ratio: lSJ/slSJ. (B) IC width - the width of the intercellular space in the region of septate junction; Septa distance – the distance between two consecutive septa; Septa thickness – the thickness of individual septa.*

In the mid-stage embryos (S13-S15), a large digestive gland primordium is filled with yolk and is progressively separated into two large lobes, which later differentiate into the first pair of digestive gland tubules. In successive developmental stages of mid-embryos, we clearly showed the formation of two distinct lobes (Fig. 4). The digestive gland epithelium forms a furrow longitudinally in the middle of the gland primordia, separating the developing lobes, and gradually extends from the ventral part of the animal towards the dorsal part and in the posterior-anterior direction. In mid-stage embryos the digestive gland lobes are still fused anteriorly and connected to the external yolk, which lies dorsally (Figs. 3A, 3A', 3B, 3B', 4A, 4B, 4C, 5A). In virtual 2D sections of stage S13 it is evident that the epithelial furrow extends approximately to the middle of the embryo (Fig. 4A). In stage S14 the furrow continues to extend anteriorly (Fig. 4B) and in stage S15 the two lobes are nearly completely separated, fused only in a small anterior area below the stomodeum (Fig. 4C).

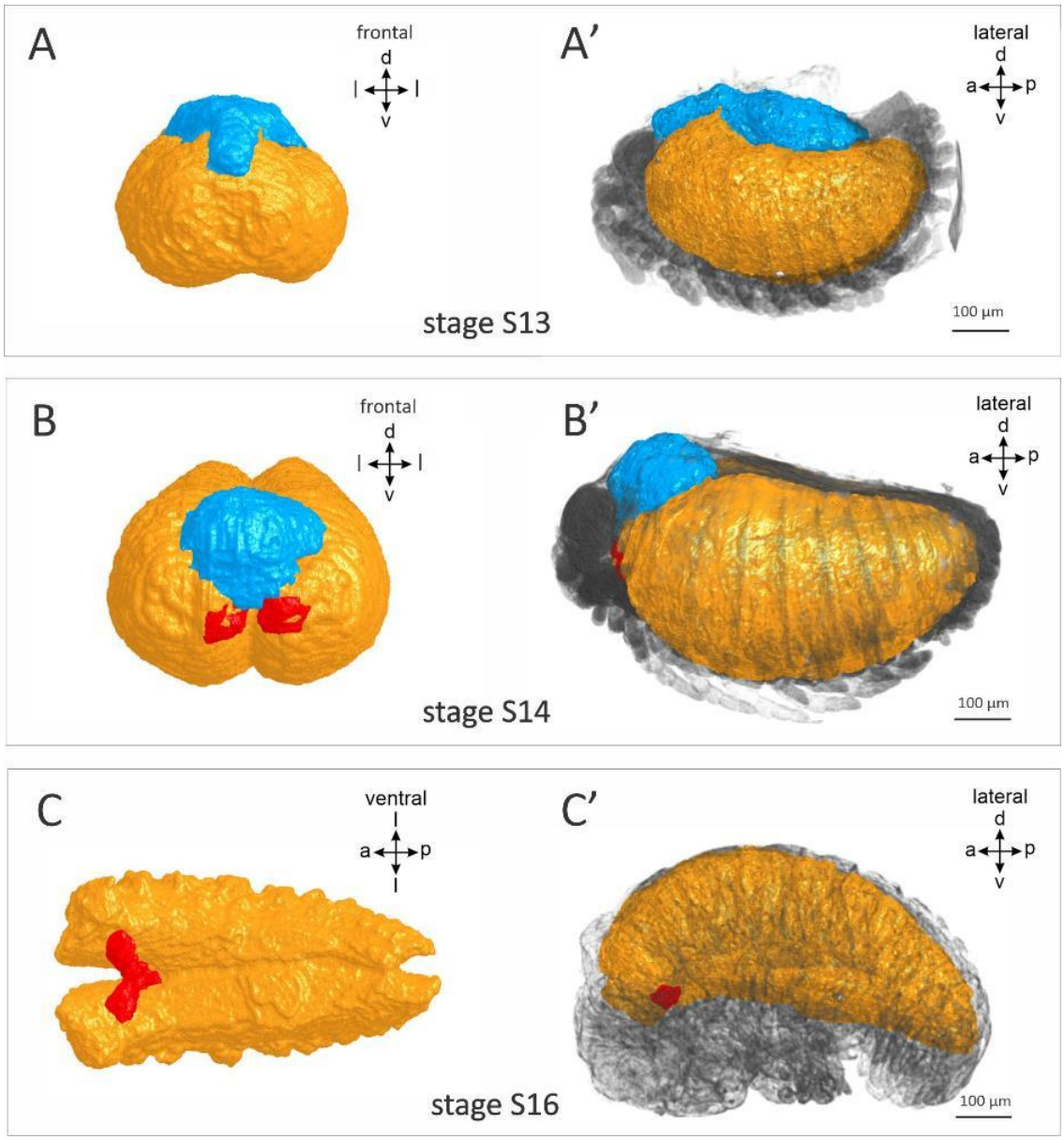

Fig. 3. *3D reconstruction of the digestive glands in P. scaber during morphogenesis in mid- and late-stage embryos using micro-CT imaging and segmentation. The 3D reconstructions of glands and external yolk in mid-stage embryos S13 (A) and S14 (B) and late-stage embryos S16 (C) are shown. The large primordium of digestive glands is separated into two large lobes in stages S13-S14 and later in stage S16 into a pair of tubules (yellow). The second pair of tubules is formed later, visible as small primordia starting in S14 embryos (red). The amount of external yolk gradually decreases during development (blue) and is completely depleted by stage S16. a – anterior, d – dorsal, l – lateral, p – posterior, v – ventral.*

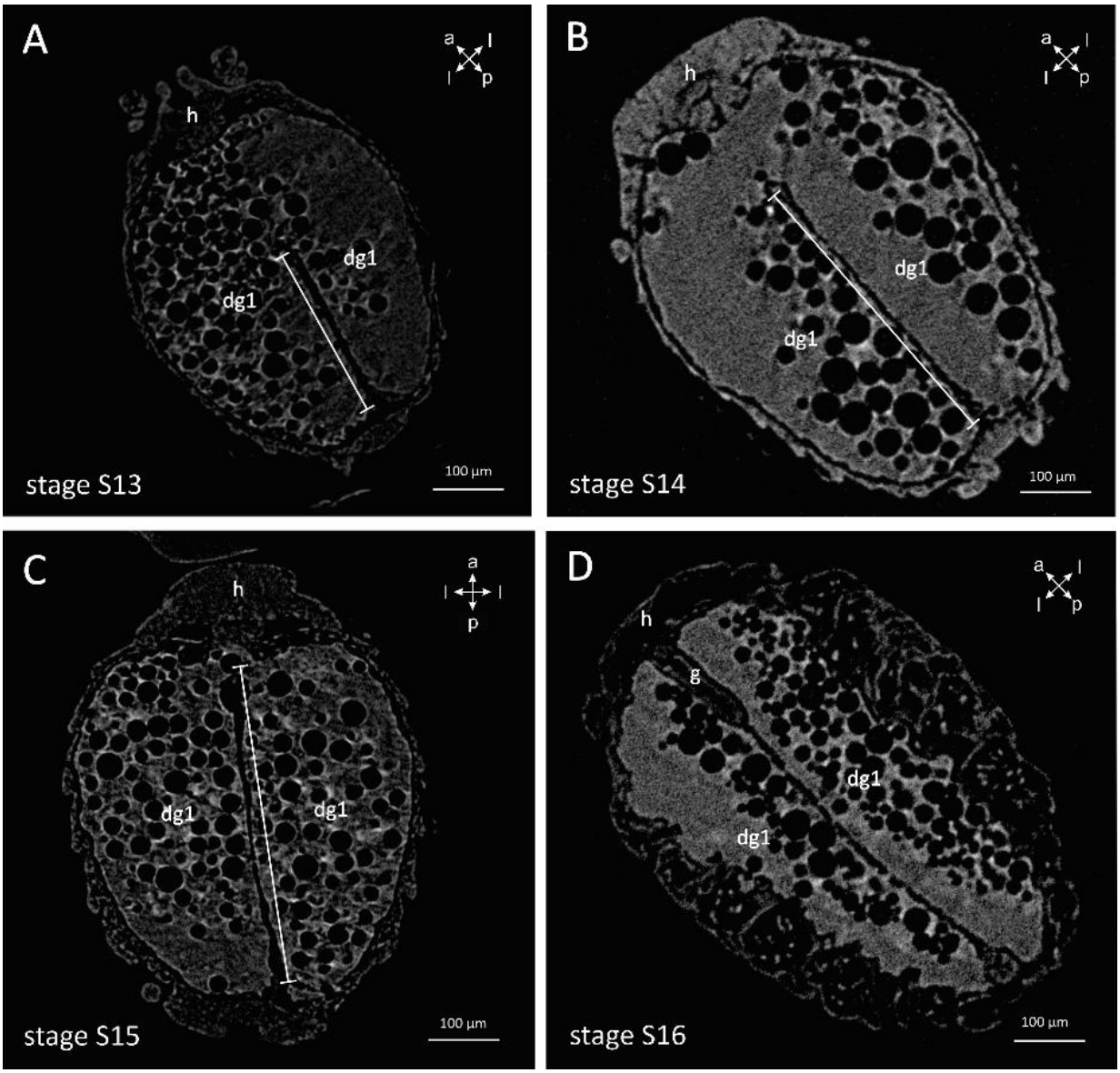

Fig. 4. *Micro-CT virtual 2D longitudinal sections of developing digestive gland tubules in different embryonic stages of P. scaber, non-osmicated samples of embryonic stages S13 (A), S14 (B), S15 (C) and S16 (D). The epithelial furrow between two developing lobes (indicated by a line) gradually elongates from posterior to anterior end and separates gland lobes filled with yolk. The yolk includes lipid droplets (round dark areas). a – anterior, dg1 – first pair of digestive gland tubules, g – gut, h – head region, l – lateral, p – posterior.*

The onset of the second pair of the gland tubules formation is evidenced in the stage S14 embryo, revealed by analysis of micro-CT projections of different orientations. By selecting the appropriate orientations of micro-CT projections, the exact position and shape of the forming tubules is shown here. The second pair of digestive gland tubules begins to form anteriorly as two small round pouches from the first pair, as observed in 3D view of stage S14 embryo after segmentation (Fig. 3B), and in virtual 2D sections of different orientations (Figs. 5A, 5A').

In late embryogenesis (S16) the lobes of digestive glands are completely separated (Fig. 4D), filled with yolk, elongated and closely aligned with the ventrally bent shape of the embryo body (Figs. 3C, 3C', 4D). The external yolk is completely depleted. Gland tubules of the second pair are small, their shape changes from pouch- to tube-shape and they gradually elongate posteriorly (Fig. 3C).

Osmicated and non-osmicated samples of embryos were prepared in addition to evaluate the effect of sample osmification on micro-CT imaging and analyses. Comparison is shown in virtual 2D images of osmicated (Figs. 5A, 5A') and non-osmicated samples (Figs. 5B, 5B') of mid-stage embryos. In the samples treated with OsO_4, lipid-rich tissues show a very strong signal. Lipid droplets as small as 10 µm are clearly visible (Figs. 5A, 5A'). A large amount of lipid droplets of various sizes within the yolk inside and

outside digestive glands is observed. The gland epithelium is clearly resolved in osmicated samples, as the cells are filled with lipid droplets. The lipid droplets in cells are smaller than those within yolk.

ELONGATION OF THE SECOND PAIR TUBULES AND WIDTH REDUCTION OF THE FIRST PAIR TUBULES DOMINATE THE DIGESTIVE GLANDS MORPHOGENESIS DURING MARSUPIAL AND POSTMARSUPIAL MANCAE DEVELOPMENT

Digestive glands are connected to digestive tract at the anterior end of the glands, which is in the first segment of the pereon, as shown by micro-CT analysis in all analyzed consecutive stages of marsupial and postmarsupial mancae (Fig. 6). In early marsupial mancae, digestive gland tubules of the first pair are filled with yolk and extend deep into the pleon. The tubules of the second pair are very short at this stage of development, reaching approximately only to the middle of the second segment of the pereon (Figs. 6A, 6A'). In the mid-stage marsupial mancae, the first pair of digestive gland tubules are of the same length as in early mancae, but are slightly narrower. The tubules of the second pair elongate considerably and extend to the fourth segment of the pereon in this stage (Figs. 6B, 6B'). In late marsupial mancae, the tubules of the first pair extend into the pleon, similar as in the earlier manca stages, but are much narrower in this stage. Tubules of the second pair extend approximately to the sixth body segment of the pereon (Figs. 6C, 6C'). In the postmarsupial mancae, the gland tubules are even narrower than in the marsupial mancae and the tubules of the second pair elongate to approximately ¾ of the length of the first pair, to the front of the pleon (Figs. 6D, 6D'). Micro-CT analyses of the digestive gland tubules in manca stages do not show the spiral shape, which is discernible in the gland tubules of adults (Fig. 9A').

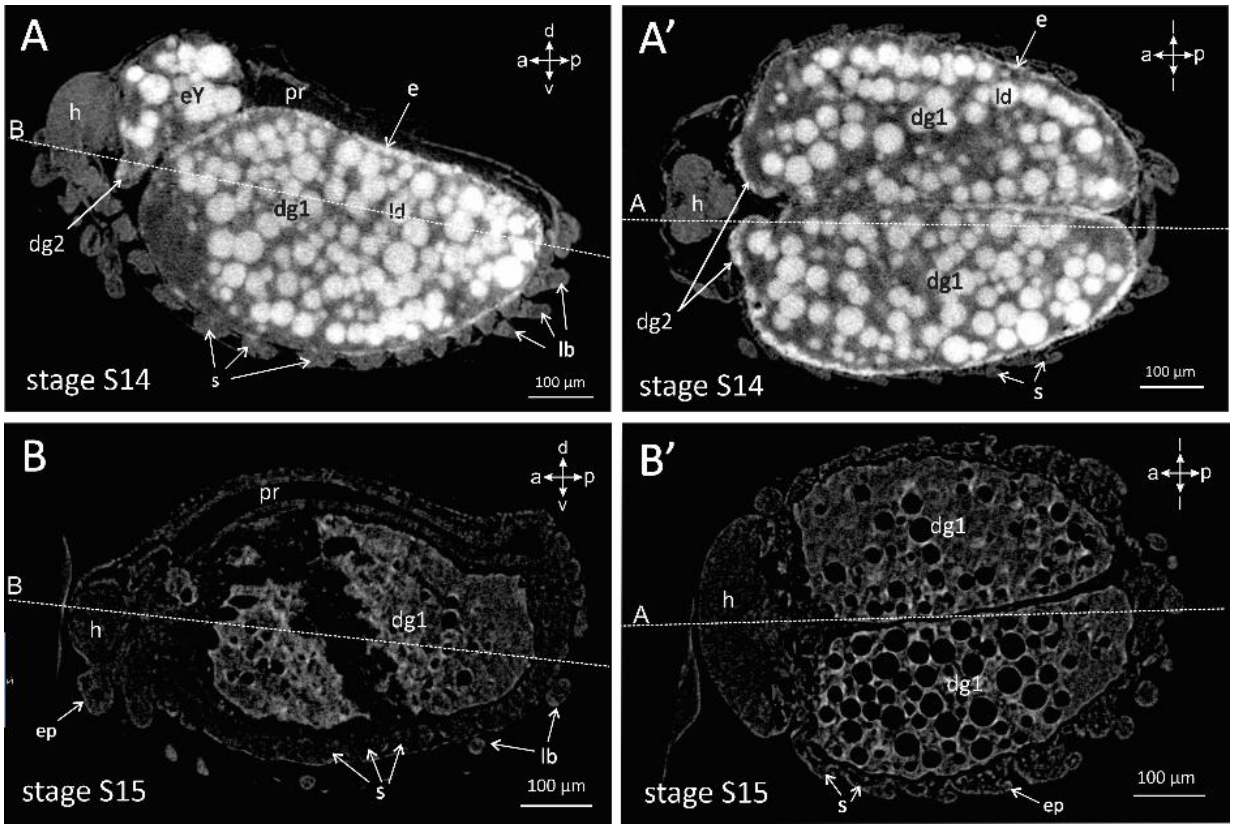

Fig. 5. *Micro-CT virtual 2D longitudinal sections of the P. scaber mid-stage embryos in the region of the developing digestive glands. The dotted lines in images indicate the location of the section shown in the adjacent image and vice versa. A, A') Stage S14, osmicated sample. The yolk includes lipid droplets (ld), which show a strong signal in osmicated specimens. The first pair of gland lobes (dg1) is divided by epithelium, while the second pair (dg2) begins to form. The digestive gland epithelium (e) is clearly discernible, containing abundant small lipid droplets. B, B') Stage S15, non-osmicated sample. Lipid droplets within yolk are recognizable as round areas with no signal. a – anterior, d – dorsal, dg1 – first pair of digestive gland tubules, dg2 – second pair of digestive gland tubules, ep – epidermis, eY – external yolk, h – head region, l – lateral, lb – limb buds, p – posterior, pr – proctodeum, s – body segments, t – tergites, v – ventral.*

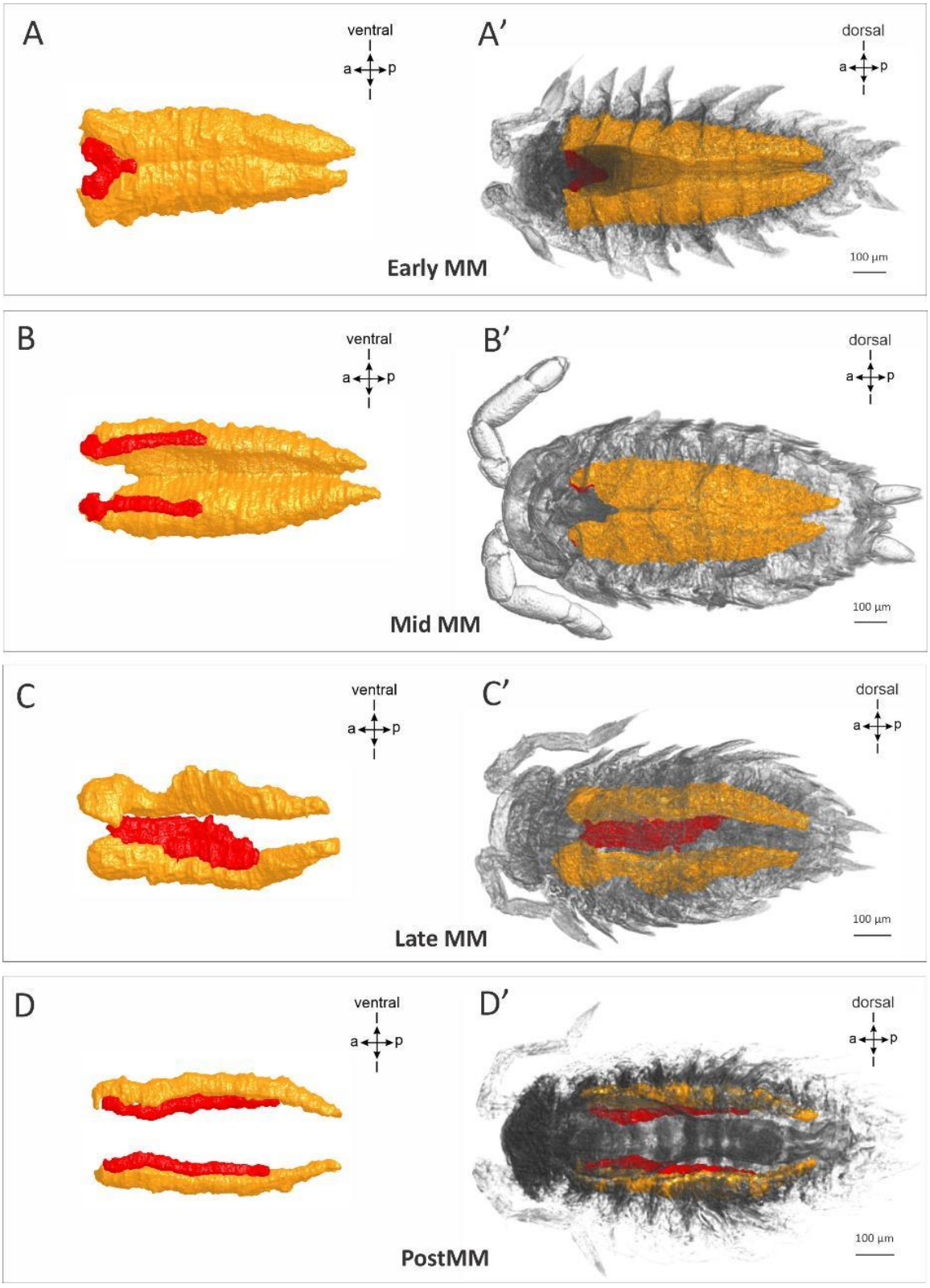

Fig. 6. 3*D reconstruction of the digestive glands in marsupial and postmarsupial mancae stages of P. scaber using micro-CT imaging and segmentation. A, A') Early marsupial manca. B, B') Mid-stage marsupial manca. C, C') Late marsupial manca. D, D') Postmarsupial manca 1 day after release from marsupium. The gland tubules of the first pair are shown in orange and are initially filled with yolk, the amount of which gradually decreases during development, evidenced as narrowing of the tubules. The gland tubules of the second pair are shown in red and gradually elongate during mancae development. a – anterior, d – dorsal, l – lateral, p – posterior, v – ventral.*

VOLUME REDUCTION OF THE DIGESTIVE GLAND LOBES AND TUBULES OF THE FIRST PAIR AND VOLUME INCREASE OF THE TUBULES OF THE SECOND PAIR DURING MORPHOGENESIS

Micro-CT enables quantification of volumes of the segmented structures. The numbers of voxels, segmented for the individual structures in the same specimen (first pair of tubules, second pair of tubules and external yolk) were available in Dragonfly software and were used to evaluate volume values in µm3 for the specific structure (Figs. 7, 8). The volume of the first pair of gland tubules is significantly reduced from stage S14 embryo to postmarsupial mancae, mostly from late embryo (S16) to marsupial manca stages (Fig. 7A). The volume of the second pair of the tubules gradually increases from stage 16 embryo throughout marsupial manca stages, and from marsupial to postmarsupial mancae no clear direction of the volume change can be determined due to specimens' variability (Fig. 7B). From stage S13 to stage S14 embryos the increase of volume of the first pair is evident, while the second pair of tubules is not present yet (Fig. 7). The second pair of tubules is present from stage S14 embryo onwards and a slight decrease of the volume to stage S16 embryo is evident (Fig. 7B), which may be due to shape change from pouch to tubule, shown in Figure 3.

The quantitative data of the digestive glands volume also demonstrate that the ratio between the volumes of the second and the first pair of gland tubules (dg2 / dg1) changes intensely during development. The ratio in general increases during development due to decrease of the first pair volume and increase of the second pair volume, except in the stage 16 embryo, in which the mean value of the ratio is lowest (1:161). In stage 14 the mean value of the ratio is approximately 1:110, in early marsupial manca 1:46, in mid-stage marsupial manca 1:18, in late marsupial manca and in postmarsupial manca approximately 1:6 (Fig. 8). The volume of the yolk outside the digestive glands (external yolk) in general decreases during mid-stage embryo development and is not present from the stage of late embryo onwards (Fig. 8).

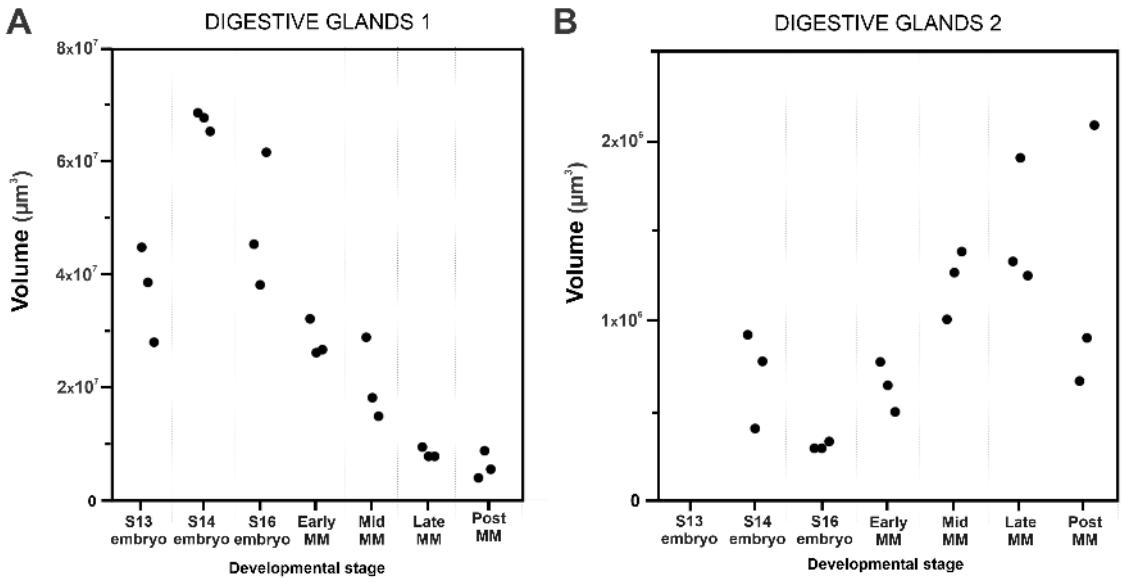

Fig. 7. *Quantitative analysis of the volumes of the first (A) and the second pair (B) of digestive gland tubules in P. scaber developmental stages: mid-stage embryo S13; mid-stage embryo S14; late-stage embryo S16; early marsupial manca (early MM); mid-stage marsupial manca (mid MM); late marsupial manca (late MM); postmarsupial manca (postMM). The data in µm3 were collected from micro-CT analysis of the whole animals, based on the number of segmented image elements (voxels). Take a notice on the different scale in the y axis in (A) in (B). Individual data obtained in three specimens of each developmental stage are shown (grey dots). A) The volume of the first pair decreases from stage S14 embryo onwards. In mid-stage embryos (S13 to S14) the volume of the first pair of digestive gland tubules increases. B) The second pair of the digestive gland tubules starts to form in mid-stage embryo S14. During marsupial manca development (early MM, mid MM, late MM) their volume gradually increases.*

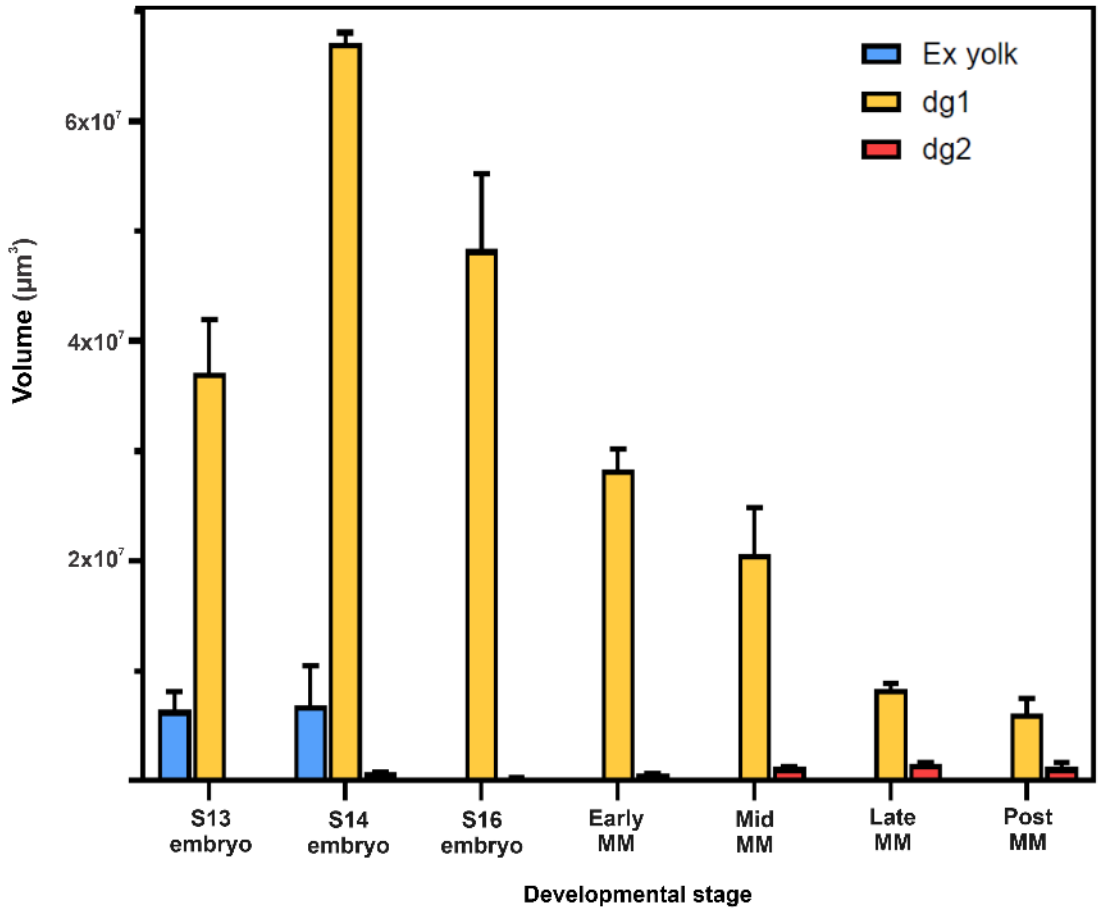

Fig. 8. *Quantitative analysis of volumes of yolk outside the glands (Ex yolk, blue) and volumes of the first and the second pairs of digestive gland tubules (dg1, yellow; dg2, red) in developmental stages of P. scaber: mid-stage embryo S13; mid-stage embryo S14; late-stage embryo S16; early marsupial manca (early MM); mid-stage marsupial manca (mid MM); late marsupial manca (late MM); postmarsupial manca (postMM). The data in µm3 were collected from micro-CT analysis of the whole animals, based on the number of segmented image elements (voxels). Each column represents the mean value of the volume (N = 3) with the standard error bar of the mean. In mid-stage embryos (S13, S14) the external yolk (blue) is still present, the volume of the first pair of digestive gland tubules (dg1, yellow) increases and in stage S14 the second pair of the digestive gland tubules (dg2, red) starts to form. In marsupial manca (early MM, mid MM, late MM) and postmarsupial manca the ratio between the volumes of dg2 and dg1 is higher than in embryos and gradually increases.*

3D MORPHOLOGY OF DIGESTIVE GLANDS IN ADULTS

3D reconstruction of adult *P. scaber* external and internal anatomy by micro-CT method clearly shows the anatomy of digestive system within organism. Digestive gland tubules extend longitudinally along the body from the first segment of pereon to the pleon and are located ventrally to digestive tract (Figs. 9A, 9B). The connection between the digestive glands and the gut is in the first segment of pereon (Fig. 9A). This is the region of the foregut - hindgut junction, where the stomach with filters and the anterior chamber with typhlosole are fused as visible in cross virtual section (Fig. 9B). The characteristic spiral shape of all four gland tubules is evidently visible in the 3D reconstruction (Fig. 9A'). The two types of cells, B and S cells, are clearly distinguished in histological sections of gland epithelium (Fig. 9C). B cells are dome-shaped and filled with lipid droplets, while S cells are wedge-shaped and contain fewer lipid droplets. Brush border is present on the apical surface of both cell types.

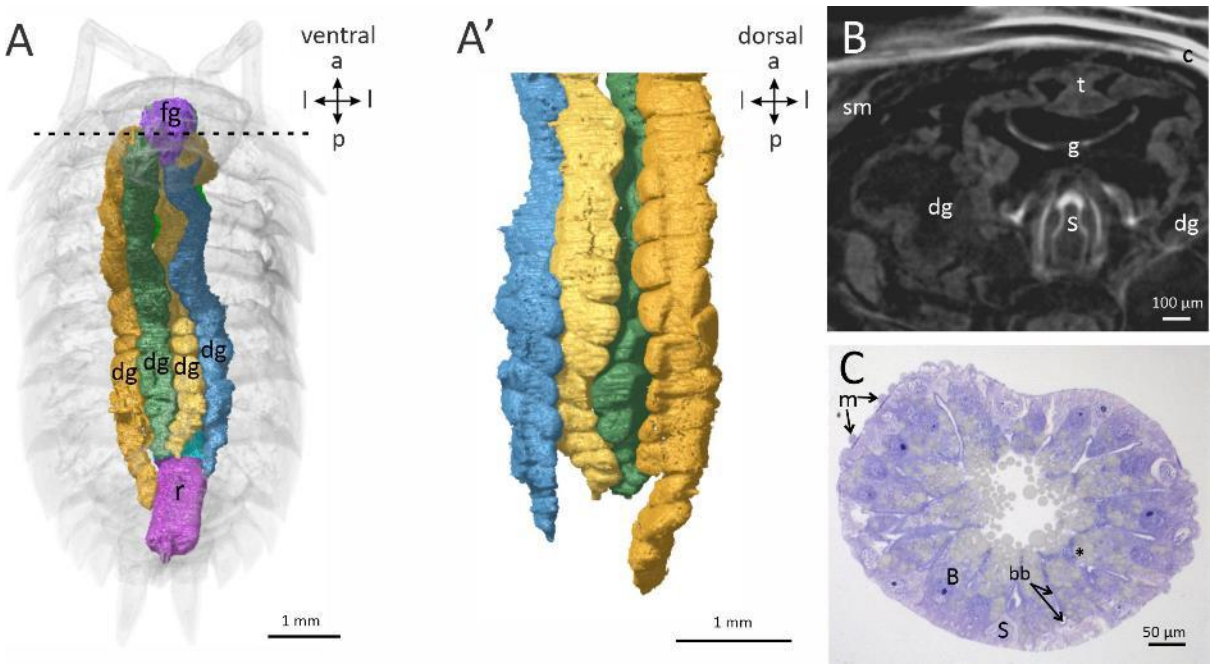

Fig. 9. *Anatomy and histology of digestive glands in P. scaber adult. A, A') 3D anatomy of the digestive system characterized by micro-CT imaging and segmentation. A) View from the ventral side of the animal, showing both pairs of tubules of the digestive glands (dg) and digestive tract dorsally to the glands. The tubules connect to the digestive tract in the region of foregut – hindgut junction. A') Dorsal view of the gland tubules. Higher magnification shows spiral shape of the digestive gland tubules. B) Micro-CT virtual 2D cross section of animal in the region marked by dotted line in A, where digestive glands (dg) connect to the gut (g), in the region of foregut – hindgut junction. The lumens of the tubules on each side of the body are fused in this region. C) Semithin section of the digestive gland tubule showing histological structure of the epithelium. The epithelium is composed of dome-shaped B cells (B) and wedge-shaped S cells (S). Muscles (m) surrounding the gland epithelium are visible. The apical surface of both cell types is differentiated into brush border (bb). There are many lipid droplets (*) in B cells. a – anterior, B – B cell, bb – brush border, dg – digestive gland tubules, c – exoskeletal cuticle, fg – foregut, g - gut, l – lateral, m – muscles of glands, n – cell nucleus, p – posterior, r – rectum, S – S cell, s – stomach, sm – skeletal muscles, t – typhlosole.*

EPITHELIAL CELLS OF DIGESTIVE GLANDS CHANGE FROM CUBOIDAL TO DOME-SHAPED B CELLS AND WEDGE-SHAPED S CELL IN LATE MARSUPIAL MANCA STAGE

Histological analysis of digestive gland epithelium during *P. scaber* embryonic and postembryonic development, from the mid-embryonic stage (S13) to the stage of postmarsupial manca, shows that cuboidal epithelial cells change to dome-shaped B cells and wedge-shaped S cells and prominent brush border is evidenced in the apical surface (Fig. 10). Digestive gland primordia in embryos are large and filled with yolk, epithelial cells are mostly cuboidal with round nuclei, cells are filled with small lipid droplets and particularly in lipid-rich regions cells bulge apically into lumen. Prominent brush border was not observed by histology and cells do not shown differentiation into the B and S cell types (Figs. 10A, 10B) that are characteristic for the digestive glands in adult animals (Fig. 9C). In early- and mid-stage marsupial mancae, yolk is still present in the lumen of digestive gland tubules. In general, epithelial cells in histological sections are similar to cells in preceding embryonic stages (Fig. 10C). Late marsupial manca is the first stage in which the two cell types, B cells and S cells, are clearly distinguished morphologically. B cells are dome-shaped and deeply protrude into the gland lumen, occupying a large part of gland volume, while S cells are small wedge-shaped cells between B cells (Fig. 10D). Lipid droplets are present mainly in B cells. The brush border is prominently visible by histology from this stage onwards. In late marsupial and postmarsupial mancae, yolk no longer fills the lumen of any of the four digestive gland tubules (Figs. 10D, 10E, 10F). In general, digestive gland epithelia of all developmental stages examined contain many lipid droplets of various sizes, except in the postmarsupial manca 14 days after release from the marsupium, in which only in individual cells small lipid droplets were observed (Fig. 10F).

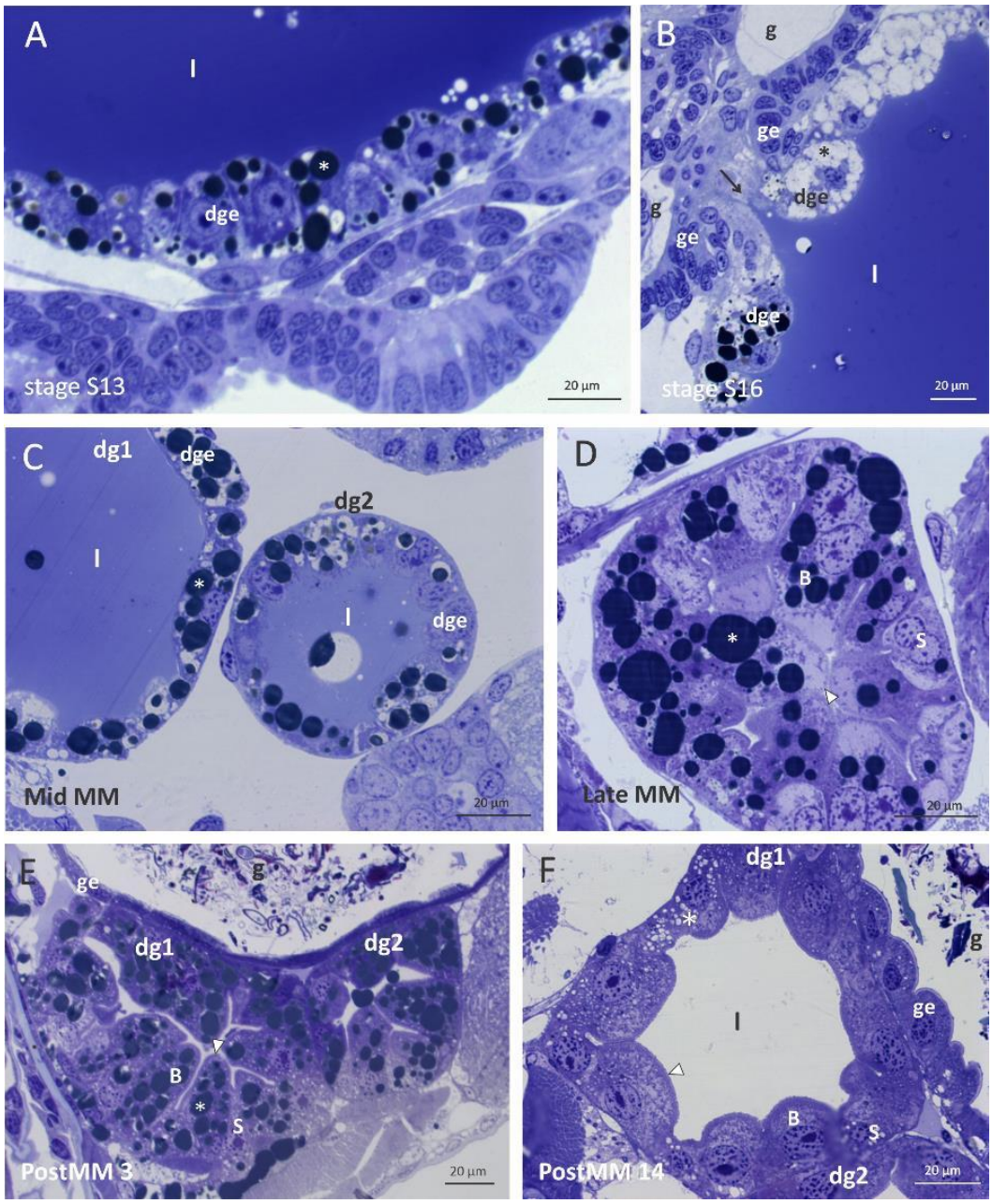

Fig. 10. *Histology of digestive gland epithelium during P. scaber embryonic (A, B), marsupial manca (C, D) and postmarsupial manca (E, F) development. A) Mid-stage embryo S13. Yolk-filled gland primordium in is surrounded by epithelium (dge) with mostly cuboidal cells filled with lipid droplets (*) and bulging in lumen (l). B) Late-stage embryo S16. The image shows connection of digestive glands to the gut (g) via hepatopancreatic duct (arrow) in the region of foregut-hindgut junction. The digestive gland epithelium is similar as in S13 and is continuous with the gut epithelium (ge). C) Mid-stage marsupial manca. Tubules of the first (dg1) and the second (dg2) pair of digestive glands include yolk in lumen and consist of epithelium (dge) with lipid droplets-filled cells bulging into lumen (l). D) Late marsupial manca. The B and S cells (B, S) are discernible, both with prominent brush border (arrowhead). B cells protrude deep into the lumen, resulting in greatly reduced lumen. Lumen is no longer filled with yolk. Lipid droplets prevail in the B cells (*). S cells are smaller with a lighter cytoplasm. E) Postmarsupial manca 3 days after release from marsupium. Both tubules (dg1 and dg2) are visible beneath the gut (g), closely apposed to each other and the gut epithelium (ge). Epithelium appears similar as in late marsupial manca, with both cell types discernible (B, S). F) Postmarsupial manca 14 days after release from marsupium. Lumen of the digestive glands is empty. Epithelial cells contain small lipid droplets that are sparse (*). B – B cell, dg1 – first pair of digestive gland tubules, dg2 – second pair of digestive gland tubules, dge – digestive gland epithelium, g – gut, ge – gut epithelium, l – gland lumen, S – S cell.*

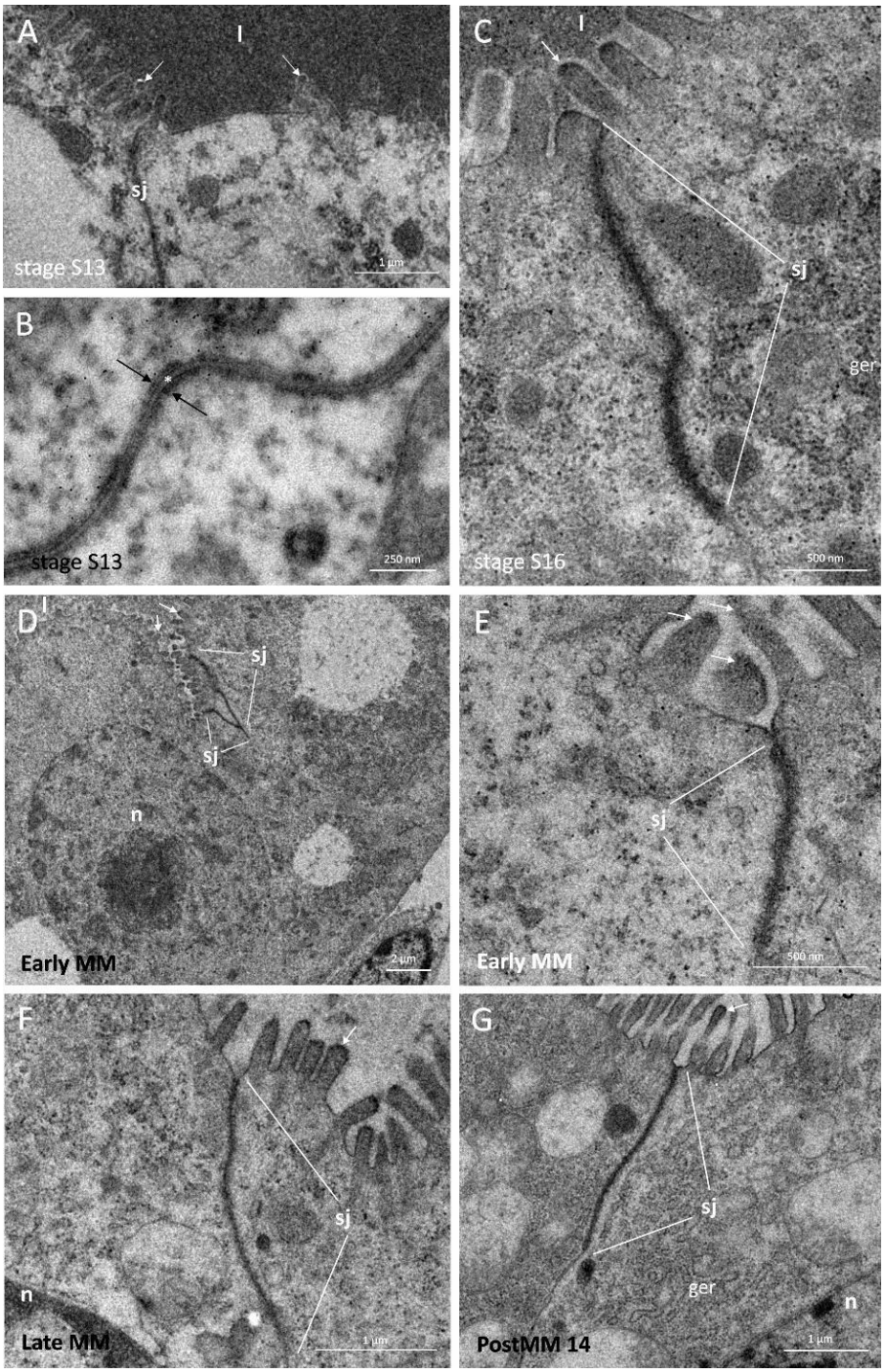

Fig. 11. *Ultrastructure of septate junctions in digestive gland epithelium of P. scaber embryonic (A, B, C), marsupial manca (D, E, F) and postmarsupial manca (G) development. A, B) Mid-stage embryo S13. Septate junction (sj) connects two neighbouring cells in the apical region, recognized as electron dense border between cells. The higher magnification in (B) shows the electron dense cytosol just beneath the lateral membranes (black arrows) and electron dense intercellular space (*), while septa are hardly discernible. The microvilli are present in S13 embryo (white arrows in A), but not over the entire apical surface, and reach into lumen full of yolk (l). C) Late-stage embryo S16. Septate junction (sj) and microvilli (white arrow) are shown. D, E) Early marsupial manca. Lower magnification in (D) shows the range of septate junction (sj) in relation to the entire border between the cells. Microvilli are abundant (white arrows). F) Late marsupial manca. Septate junction (sj) is long, and microvilli are abundant (white arrow). Note that the gland lumen is devoid of yolk. G) Postmarsupial manca 14 days after release from marsupium. Long septate junction (sj) and long and abundant microvilli (white arrow) are observed. ger – granular endoplasmatic reticulum, l – gland lumen, sj – septate junction, n – nucleus.*

SEPTATE JUNCTIONS BETWEEN CELLS OF DIGESTIVE GLAND EPITHELIUM ELONGATE CONSIDERABLY DURING DEVELOPMENT FROM EMBRYOS TO POSTMARSUPIAL MANCAE

The formation of septate junctions enables barrier and transport functions of epithelium, which must be established during gland morphogenesis, so the evaluation of the ultrastructure of septate junctions is an important part of the study of digestive glands morphogenesis. In the endodermal epithelia, smooth septate junctions are located immediately subapically. Septate junctions are discernible as electron dense septa array in the intercellular space between the lateral membranes of neighbouring cells. The neighbouring plasma membranes are evenly spaced in the junction region (Fig. 11). We have analysed the ultrastructure of septate junctions in epithelium of digestive gland primordia of embryos and in the epithelium of digestive gland tubules in the marsupial and postmarsupial manca stages and in adults.

In the epithelium of the digestive glands, smooth septate junctions are visible subapically between the lateral membranes of epithelial cells in all analysed developmental stages, i.e., from the mid-stage embryo in stage S13 onwards (Fig. 11). In all analysed developmental stages, the septate junctions show similar ultrastructure. The lateral membranes run parallel, without significant expansion of the intercellular space. The septa are often hardly or even not discernible due to sectioning orientation, but the junction and its length can be determined by electron density of intercellular space and cytosolic regions next to membranes and by perfectly parallel course of both membranes (Fig. 11)

Measurements of the length of septate junctions (lSJ) showed that septate junctions in the digestive glands elongate during animal development (Fig. 12A). The median length of septate junctions is around 1.3 μm in the embryonic stages, 1.7 μm in the marsupial manca stages, and 2.5 μm in the postmarsupial stages, while in adults the septate junctions are around 2.6 μm long. Septate junctions are straight to slightly folded (Fig. 11) and the linearity index do not change much during development (Fig. 12B). The values of INSJ are lower than in adult animals, which means that the membranes in the developmental stages are less folded than in adults (Fig. 12B).

The sections of septate junctions are rarely transverse enough to discern clearly the ultrastructure of detailed characteristics of septate junction. Nevertheless, we obtained data on the width of the intercellular space in the region of septate junctions, the distance between consecutive septa in septate junctions and the thickness of individual septa, and compared the ultrastructure of septate junctions between embryos, marsupial mancae and adults. The width of the intercellular space does not change significantly during development (embryos and marsupial mancae) and is similar as in adults. The median values are 16.3 nm in embryos, 17.0 nm in marsupial mancae and 17.0 nm in adults. The values of the width of the intercellular space are less variable in adults (Fig. 13A). The distance between consecutive septa in septate junctions is slightly shorter in embryos/marsupial mancae (median value 5.1 nm) than in adults, with median 6.6 nm (Fig. 13B). The thickness of septa is similar in embryos/marsupial mancae (median value is 4.3 nm) and in adults, with median value 5.2 nm. (Fig. 13C).

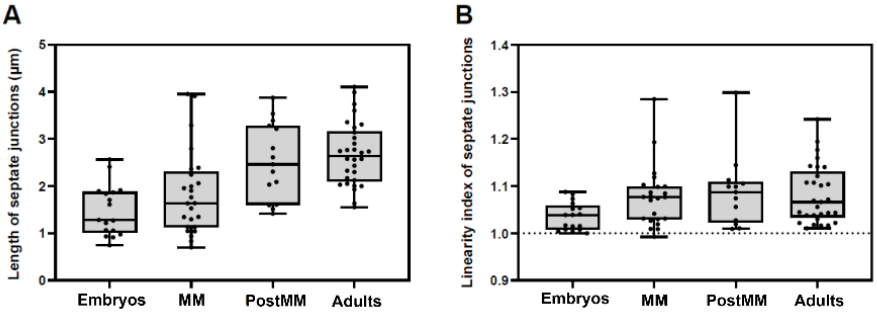

Fig. 12. *Morphometrical analysis of septate junction length and linearity index in the digestive gland epithelium in P. scaber embryos, marsupial mancae, postmarsupial mancae and adult animals. The data are graphically represented by box plots with whiskers. Individual data are shown as dots. A) The length of septate junctions increases from embryos to marsupial mancae and postmarsupial mancae and to adults, with the highest increase from marsupial to postmarsupial development. B) The linearity index of the septate junction (INSJ), calculated as length of the SJ / length of the SJ straight line, do not change drastically during development. The data show that septate junctions are slightly more folded during postembryonic development and in adults than during embryonic development (higher linearity index).*

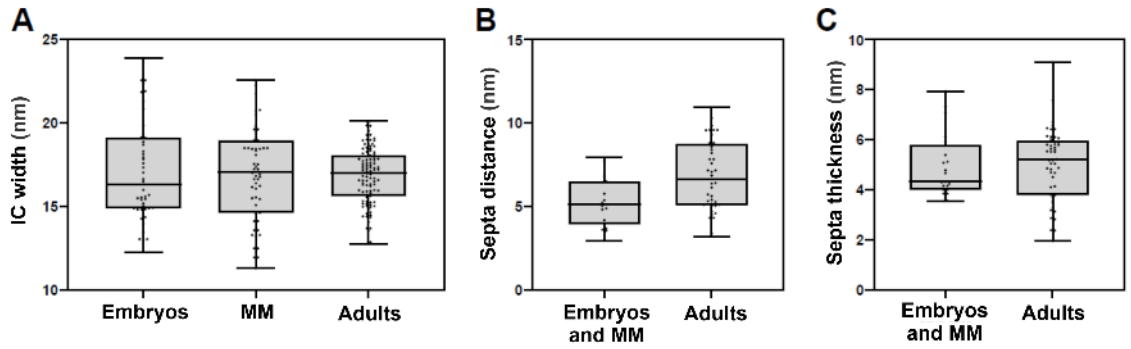

Fig. 13. *Morphometrical analysis of ultrastructural characteristics of septate junctions in the digestive gland epithelium in P. scaber embryos, marsupial mancae (MM) and adult animals. The data are graphically represented by box plots with whiskers. Individual data are shown as dots. A) The width of intercellular space (IC width) in the region of septate junction is similar in embryos and marsupial mancae and in adults. The values are more variable in developmental stages than in adults. B) The distance between consecutive septa is slightly shorter in developmental stages (embryos and marsupial mancae) than in adults. C) The thickness of individual septa is similar in embryos and marsupial mancae than in adults.*

DISCUSSION

Multiscale and 3D imaging is indispensable to reveal structure from the organ to the cellular level and to obtain an integrative insight into the morphology of an organism as a whole. A complementary approach using light microscopy, electron microscopy and modern 3D imaging techniques (e.g. micro-CT) provides a more comprehensive insight into the internal structure of animals and a better understanding of morphology and functionality at the organizational levels of organs, tissues, and cells, which is particularly valuable in studies of organ and tissue morphogenesis (Castejon *et al.*, 2018; Spitzner *et al.*, 2018; Castejon *et al.*, 2021). Here, we present implementation of multiscale imaging and morphometry to characterize morphogenesis of digestive glands during embryonic and postembryonic development of isopod crustacean *P. scaber*, showing the importance of integration of the information obtained by different imaging techniques (micro-CT, histology, TEM), supplemented by quantification of the specific features of interest in the selected developmental stages, such as digestive glands' volume and ultrastructural characteristics of septate junctions.

Specimen preparation was successfully adjusted and effective micro-CT imaging of the internal and external anatomy of very small samples was achieved in the study presented here. All organs of the digestive system and their distribution inside the organism are clearly visible on virtual 2D sections and simultaneously the external morphology of the organism is evident due to sufficient contrast of exoskeleton. The micro-CT method applied allowed us to accurately characterize the 3D anatomy of digestive glands in relation to other organs inside the whole organism as small as 0.8 mm (embryos) or 1-2 mm (mancae). One of the important advantages of micro-CT method is that morphology of organs and tissues can be analysed on virtual 2D sections in different orientations in correlation to 3D anatomy, which facilitates the analysis of corresponding histological structure sectioned in a specific orientation. In general, virtual 2D sections of animals obtained by micro-CT reveal the basic morphology due to differential tissue density (Baird and Taylor, 2017), which in our case was sufficient to distinguish the digestive gland epithelium and other tissues in osmicated and non-osmicated samples without the application of additional contrasting agents (e.g. Lugol's iodine or phosphotungstic acid). In the course of tissue segmentation in micro-CT analysis, we can navigate through virtual sections of the sample, which allows us to follow individual structures from different perspectives and characterize morphology more completely. Previous knowledge of the investigated sample structure acquired from classical histological analyses has proven to be valuable for accurate and effective identification of organs and tissues in the data obtained by micro-CT. Histological analysis provides additional, a more detailed information due to better spatial resolution of light microscopy compared to micro-CT and different staining procedures employed, which can give contrast to specific features of the sample (du Plessis *et al.*, 2017; O'Sullivan *et al.*, 2018), clearly showing tissue structure, epithelial morphology, and shape and basic structure of the cells. Histological analysis in our study revealed the information on cell shape changes during differentiation, the amount and size of lipid droplets and formation of the prominent brush border. Our experience confirms that it is essential to combine micro-CT with histology to obtain comprehensive information at all levels from the organism to the cells and to facilitate analysis with micro-CT.

We have evaluated the effect of sample osmification on micro-CT imaging and analyses. All samples were fixed in aldehydes, dehydrated in ethanol series and

dried after HMDS treatment, and in addition, a subset of samples was contrasted with OsO_4 before dehydration. In both, osmicated and non-osmicated samples, the anatomy of the embryos and mancae was well preserved and we obtained adequate contrast and resolution for successful segmentation and 3D imaging of organs and tissues. In the osmicated samples, tissues containing lipids showed a very strong signal, which is due to osmium tetroxide binding to lipids. Osmium is a transition metal and gives high attenuation of x-rays and reduced transmittance in micro-CT analysis (O'Sullivan *et al.*, 2018). The contrast and resolution achieved with this method enable detailed visualization of lipid droplets and facilitate quantitative analysis of their number and size, which is valuable for many studies involving lipid droplets analysis. In the osmicated samples of *P. scaber* embryos and marsupial mancae lipid droplets show a very strong signal and are clearly imaged within the external yolk, within the yolk in the lumen of digestive gland lobes and in the epithelium lining the digestive glands. The yolk outside the glands (external yolk) and the yolk incorporated in the gland lumen are different in structure, external yolk forms large clusters visible by stereomicroscope (Wolff, 2009; Milatovič *et al.*, 2010). Gradual incorporation of yolk into glands' lumen during embryonic development is characteristic for the peracarid species studied previously (Browne *et al.*, 2005; Wolff, 2009; Milatovič *et al.*, 2010; Manship *et al.*, 2011), while in decapods the digestive glands are much less prominent during development and were not reported to contain yolk (Vogt, 2008; Spitzner *et al.*, 2018; Štrus *et al.*, 2019; Kalacheva *et al.*, 2023).

Results of micro-CT analysis in this study upgrade and complement previous data on the embryonic and postembryonic development and morphology of the digestive system of *P. scaber* (Štrus *et al.* 2008; Wolff, 2009; Milatovič *et al.*, 2010; Štrus *et al.*, 2019), that were based on light microscopy, fluorescence microscopy and scanning electron microscopy. Studies of Wolff (2009) and Milatovič *et al.* (2010) highlight that two useful characters for distinguishing the sequential developmental stages of *P. scaber* are the size and shape of the digestive glands. Here we provide a detailed insight into the internal 3D anatomy of the embryonic and postembryonic developmental stages of *P. scaber* and a quantitative imaging of digestive glands morphogenesis in the context of whole animals during development. In mid-stage embryos, 3D reconstructions reveal a large primordium of the digestive glands, that afterwards divides into two distinct lobes during mid-embryonic development by epithelium progressively forming the furrow in the ventral-dorsal and posterior-anterior directions. As observed here by histology, the epithelial cells enclosing the glands are cuboidal in shape in the mid-stage and late embryos as well as in the mid-stage marsupial mancae. Cells bulge in the gland lumen and contain small lipid droplets. Distinct dome-shaped B and wedge-shaped S cells are morphologically distinguished in the late marsupial manca stage. Orange autofluorescence, characteristic for S cells in adults under ultraviolet excitation (Žnidaršič *et al.*, 2005), was previously recorded already in embryos (Štrus *et al.*, 2008), thus we assume that certain aspects of functional and ultrastructural differentiation precede cell shape modification during morphogenesis.

Using different projections of 3D reconstruction and virtual 2D sections of embryos obtained by micro-CT imaging, we have characterized the formation of the second pair of gland tubules in detail. Gland tubules of the second pair firstly appear as two small outgrowths, originating anteriorly from the first pair in mid-stage embryo S14. In the study by Milatovič *et al.* (2010), the formation of the second pair was first observed with a stereomicroscope in stage S15. By micro-CT 3D reconstruction and volume quantification we have clearly shown the progress of the second pair of digestive gland tubules elongation in the anterior-posterior direction alongside the first pair and gradual increase of their volume during late embryo, marsupial manca and postmarsupial manca development. Concurrently with the second pair of digestive glands tubules elongation, the volume of the first pair of gland tubules gradually decreases due to narrowing of the tubules. Combination of micro-CT and histological analysis showed that volume decrease and shape change are a consequence of yolk consumption and lumen reduction. Complete depletion of yolk within gland lumen in late marsupial manca stage coincides with morphological differentiation of B and S cells observed by histology as cell shape modification. In this stage mancae do not feed due to moulting, but by the start of feeding soon after release from marsupium the full functionality of the manca digestive glands is necessary. B cells of both pairs of gland tubules incorporate a high amount of different-sized lipid droplets in all developmental stages of *P. scaber* investigated, except in postmarsupial mancae 14 day after release. Abundant lipid droplets are characteristic for B cells in adult isopods and R cells in adults and larval decapods (Biesiot and McDowell, 1995; Nishida *et al.*, 1995; Vogt, 2008; Štrus *et al.*, 2019). The 14 days postmarsupial mancae have less abundant and smaller lipid droplets in digestive gland epithelium, which can be attributed to animal physiological or nutritional condition (moulting), and not necessarily to the developmental stage. There are studies of adult isopods showing that after the food shortage the lipid droplets in digestive glands' cells are less abundant and smaller (Štrus *et al.*, 1985; Lešer *et al.*, 2008).

Quantification of the length of septate junctions in digestive gland epithelium in *P. scaber* showed that septate junctions gradually elongate during development from embryonic stages to postmarsupial manca stages. The results suggest that the paracellular barrier function of the digestive gland epithelium is basically established

in the investigated stages of embryos and mancae. In these developmental stages, yolk is consumed by the gland cells and individual microvilli are already evident apically. Yolk is completely depleted by the late marsupial manca stage, when moulting of manca occurs. The most intense increase of the septate junctions' length was evident at transition from marsupial to postmarsupial manca stage, which corresponds to release of the animal from marsupium to the external environment. In postmarsupial mancae the septate junctions are pronouncedly elongated and are only slightly shorter than in adult animals, which coincides with food source change and animal feeding on external nutrient sources. Quantification of ultrastructural characteristics of septate junctions further showed that the width of the intercellular space in the region of septate junctions and the thickness of septa are similar in embryos, marsupial manca stages and in adults, while the distance between consecutive septa is slightly larger in adults.

There is not much data available on septate junction differentiation during digestive system morphogenesis. Two comprehensive studies that analysed the ultrastructure of septate junctions in digestive system of more than two developmental stages were performed on different epithelia in *Drosophila melanogaster* by Tepass and Hartenstein (1994) and on *P. scaber* hindgut epithelium by Bogataj *et al.* (2019). Tepass and Hartenstein (1994) showed that septate junctions in midgut epithelium of *D. melanogaster* are differentiated only in the first larval stage. In *P. scaber* hindgut the septate junctions are gradually differentiated and elongated during development, with shorter septa arrays in late embryos than in manca stages. In postmarsupial mancae 14 days after release from marsupium, septate junctions in hindgut resemble those in adults (Bogataj *et al.*, 2019). A similar sequence of septate junctions' formation as in hindgut was reported also in *P. scaber* epidermis (Kunčič *et al.*, 2022). The Sonakowska-Czajka *et al.* (2021) study of midgut differentiation in two larval stages in decapod Neocaridina davidi reported on the presence of the septate junctions in zoea I and zoea II midgut and proximal region of hepatopancreas, but the detailed ultrastructure of the junctions was not analysed. These studies reported on diverse timing of septate junction differentiation, but were performed on epithelia with different functions and in different species.

In conclusion, the advance of our study is the elucidation of digestive glands morphogenesis during embryonic and postembryonic development by integration of data obtained from multiscale imaging at organism, organ, tissue and cellular levels. Histological observations of digestive gland epithelium modifications and ultrastructural analysis of septate junctions were placed into a broader spatial context of the 3D anatomy of the digestive glands and the whole animal provided by micro-CT. In addition, morphometry showed distinct modifications of digestive glands volume and septate junctions characteristics during glands morphogenesis, which were correlated to the key events during animal development.

ACKNOWLEDGEMENTS

This study was funded by Slovenian Agency for Research and Innovation (ARIS) through the core program Integrative Zoology and Speleobiology P1-0184 and supported by the infrastructural center "Microscopy of biological samples", (MRIC UL, I0-0022-0481-07) of Biotechnical Faculty, University of Ljubljana.

DATA AVAILABILITY

Research data of this study were deposited at Zenodo and are available in https://doi.org/10.5281/zenodo.19369446 (images) and https://doi.org/10.5281/zenodo.19369681 (morphometrical data).

REFERENCES

Abrunhosa F, Kittaka J (1997). Morphological changes in the midgut, midgut gland and hindgut during the larval and postlarval development of the red king crab Paralithodes camtschaticus. Fish Sci 63:746-54. https://doi.org/10.2331/fishsci.63.746

Baird E, Taylor G (2017). X-ray micro computed-tomography. Curr Biol 27:R289-R291. https://doi.org/ 10.1016/j.cub.2017.01.066

Bettica A, Shay M, Vernon G, Witkus R (1984). An ultrastructural study of cell differentiation and associated acid phosphatase activity in the hepatopancreas of Porcellio scaber. In: Sutton SL, Holdich DM, eds. Symposia of the Zoological Society of London, 1983 Jul 7-8; Leeds, United Kingdom. United Kingdom: Clarendon Press, 199-215.

Biesiot PM, McDowell JE (1995). Midgut-gland development during early life-history stages of the American lobster Homarus americanus. J Crust Biol 15:679-85. https://www.jstor.org/stable/1548817

Brezovjakova H, Tomlinson C, Mohd Naim N, Swiatlowska P, Erasmus JC, Huveneers S, Gorelik J, Bruche S, Braga VM (2019). Junction Mapper is a novel computer vision tool to decipher cell-cell contact phenotypes. Elife 8:e45413. https://doi.org/10.7554/eLife.45413

Bogataj U, Mrak P, Štrus J, Žnidaršič N (2019). Ultrastructural differentiation of plasma membrane and cell junctions in the hindgut cells is synchronized with key

developmental transitions in Porcellio scaber. Arthropod Struct Dev 50:78-93. https://doi.org/10.1016/j.asd.2019.04.004

Browne WE, Price AL, Gerberding M, Patel NH (2005). Stages of embryonic development in the amphipod crustacean, Parhyale hawaiensis. Genesis 42:124-49. https://doi.org/10.1002/gene.20145

Castejon D, Rotlland G, Ribes E, Dufort M, Guerao G (2018). Morphology and ultrastructure of the esophagus during the ontogeny of the spider crab Maja brachydactyla (Decapoda, Brachyura, Majidae). J Morphol 279:710-23. https://doi.org/10.1002/jmor.20805

Castejón D, Rotllant G, Ribes E, Durfort M, Guerao G (2021). Description of the larval and adult hindgut tract of the common spider crab Maja brachydactyla Balss, 1922 (Brachyura, Decapoda, Malacostraca). Cell Tissue Res 384:703-20. https://doi.org/10.1007/s00441-021-03446-3

Diaz AC, Fernandez Gimenez AV, Velurtas SM, Fenucci JL (2008). Ontogenetic changes in the digestive system of Pleoticus muelleri (Decapoda, Penaeoidea). Invertebr Reprod Dev 52:1-12. https://doi.org/10.1080/07924259.2008.9652266

du Plessis A, Broeckhoven C, Guelpa A, le Roux SG (2017). Laboratory x-ray micro-computed tomography: a user guideline for biological samples. Gigascience 6:gix027. https://doi.org/10.1093/gigascience/gix027

Hames C, Hopkin S (1989). The structure and function of the digestive system of terrestrial isopods. J Zool 217:599-627. https://doi.org/10.1111/j.1469-7998.1989.tb02513.x

Handschuh S, Baeumler N, Schwaha T, Ruthensteiner B (2013). Correlative approach for combining microCT, light and transmission electron microscopy in a single 3D scenario. Front Zool 10:44. https://doi.org/10.1186/1742-9994-10-44

Izumi Y, Furuse M (2014). Molecular organization and function of invertebrate occluding junctions. Semin Cell Dev Biol 36:186-93.
https://doi.org/10.1016/j.semcdb.2014.09.009

Jonusaite S, Donini A, Kelly SP (2016). Occluding junctions of invertebrate epithelia. J Comp Physiol B 186:17-43. https://doi.org/10.1007/s00360-015-0937-1

Kalacheva NV, Ginanova TT, Kamenev YO, Maslennikov SI, Dolmatov IY (2024). Morphology and ultrastructure of digestive system in pre-zoea and zoea I larvae of red king crab, Paralithodes camtschaticus (Tilesius, 1815). Cell Tissue Res 395:1-20. https://doi.org/10.1007/s00441-023-03843-w

Kunčič K, Mrak P, Žnidaršič N (2022). Formation and remodelling of septate junctions in the epidermis of isopod Porcellio scaber during development. Zookeys 1101:159-81. https://doi.org/10.3897/zookeys.1101.78711

Lešer V, Drobne D, Vilhar B, Kladnik A, Žnidaršič N, Štrus J (2008). Epithelial thickness and lipid droplets in the hepatopancreas of Porcellio scaber (Crustacea: Isopoda) in different physiological conditions. Zoology 111:419-32. https://doi.org/10.1016/j.zool.2007.10.007

Lovett DL, Felder DL (1989). Ontogeny of gut morphology in the white shrimp Penaeus setiferus (Decapoda, Penaeidae). J Morphol 201:253-72. https://doi.org/10.1002/ jmor.1052010305

Manship BM, Walker AJ, Davies AJ (2011). Brooding and embryonic development in the crustacean Paragnathia formica (Hesse, 1864) (Peracarida: Isopoda: Gnathiidae). Arthropod Struct Dev 40:135-45. https://doi.org/10.1016/j.asd.2010.12.004

Melzer RR, Spitzner F, Šargač Z, Hornig MK, Krieger J, Haug C, Haug JT, Kirchhoff T, Meth R, Torres G, Harzsch S (2021). Methods to study organogenesis in decapod crustacean larvae II: analysing cells and tissues. Helgol Mar Res 75:2. https://doi.org/10.1186/s10152-021-00547-y

Milatovič M, Kostanjšek R, Štrus J (2010). Ontogenetic development of Porcellio scaber: staging based on microscopic anatomy. J Crust Biol 30:225–35. https://doi.org/10.1651/09-3189.1

Mrak P, Žnidaršič N, Tušek-Žnidarič M, Klepal W, Gruber D, Štrus J (2012). Egg envelopes and cuticle renewal in Porcellio embryos and marsupial mancas. Zookeys 176:55-72. https://doi.org/10.3897/zookeys.176.2418

Muhammad F, Zhang ZF, Shao MY, Dong YP, Muhammad S (2012). Ontogenesis of digestive system in Litopenaeus vannamei (Boone, 1931) (Crustacea: Decapoda). Ital J Zool 79:77–85. https://doi.org/10.1080/11250003.2011.590534

Nishida S, Takahashi Y, Kittaka J (1995). Structural changes in the hepatopancreas of the rock lobster, Jasus edwardsii (Crustacea: Palinuridae) during development from the puerulus to postpuerulus. Mar Biol 123:837–44. https://doi.org/10.1007/BF00349128

O'Sullivan JDB, Behnsen J, Starborg T, MacDonald AS, Phythian-Adams AT, Else KJ, Cruickshank SM, Withers PJ (2018). X-ray micro-computed tomography (μCT): an emerging opportunity in parasite imaging. Parasitology 145:848-54. https://doi.org/10.1017/S0031182017002074

Otani T, Ichii T, Aono S, Takeichi M (2006). Cdc42 GEF Tuba regulates the junctional configuration of simple epithelial cells. J Cell Biol 175:135-46. https://doi.org/10.1083/jcb.200605012

Rouka E, Gourgoulianni N, Lupold S, Hatzoglou C, Gourgoulianis K, Blanckenhorn WU, Zarogiannis SG

(2021). The Drosophila septate junctions beyond barrier function: Review of the literature, prediction of human orthologs of the SJ-related proteins and identification of protein domain families. Acta Physiol 231:e13527. https://doi.org/10.1111/apha.13527

Rudraiah PS, Camacho R, Fernandez-Rodriguez J, Fixler D, Grimm J, Gruber F, Kalaš M, Kremslehner C, Kuntner C, Kuzdas-Wood D, Lindblad J, Mannheim JG, Marchetti-Deschmann M, Paul-Gilloteaux P, Sampaio P, Sandbichler P, Sartori-Rupp A, Sladoje N, Verkade P, Walter A, Zoratto S (2024). Correlated multimodal imaging in life sciences: lessons learnt. Front Biomater Sci 3:1338115. https://doi.org/10.3389/fbiom.2024.1338115

Sonakowska-Czajka L, Śróbka J, Ostróżka A, Rost-Roszkowska M. (2021). Postembryonic development and differentiation of the midgut in the freshwater shrimp Neocaridina davidi (Crustacea, Malacostraca, Decapoda) larvae. J Morph 282:48-65. https://doi.org/10.1002/jmor.21281

Spitzner F, Meth R, Krüger C, Nischik E, Eiler S, Sombke A, Torres G, Harzsch S (2018). An atlas of larval organogenesis in the European shore crab Carcinus maenas L. (Decapoda, Brachyura, Portunidae). Front Zool 15:27. https://doi.org/10.1186/s12983-018-0271-z

Storch V (1984). The influence of nutritional stress on the ultrastructure of the hepatopancreas of terrestrial isopods. Symp Zool Soc Lond 53:167-84.

Storch V, Štrus J (1989). Microscopic anatomy and ultrastructure of the alimentary canal in terrestrial isopods. Monit Zool Ital Monogr 4:105-26.

Štrus J, Burkhardt P, Storch V (1985). The ultrastructure of the midgut glands in Ligia italica under different nutritional conditions. Helgoland Wiss Meer 39:367-74. https://doi.org/10.1007/BF01987408

Štrus J, Drašlar K (1988). Ultrastructural evidence of the midgut cells in the isopod Ligia italica (Isopoda: Crustacea). Inst Phys Conf Ser 93:149-50.

Štrus J, Drobne D, Ličar P, Alikhan M (1995). Comparative anatomy and functional aspects of the digestive system in amphibious and terrestrial isopods (Isopoda: Oniscidea). In: Alikhan MA, ed. Terrestrial Isopod Biology. Rotterdam: A. A. Balkema 15-23.

Štrus J, Klepal W, Repina J, Tušek-Žnidarič M, Milatovič M, Pipan Z (2008). Ultrastructure of the digestive system and the fate of midgut during embryonic development in Porcellio scaber (Crustacea: Isopoda). Arthropod Struct Dev 37:287-98. https://doi.org/10.1016/j.asd.2007.11.004

Štrus J, Žnidaršič N, Mrak P, Bogataj U, Vogt G (2019). Structure, function and development of the digestive system in malacostracan crustaceans and adaptation to different lifestyles. Cell Tissue Res 377:415-443. https://doi.org/10.1007/s00441-019-03056-0

Tepass U, Hartenstein V (1994). The development of cellular junctions in the Drosophila embryo. Dev Biol 161:563-96. https://doi.org/10.1006/dbio.1994.1054

Torres G, Melzer RR, Spitzner F, Šargač Z, Harzsch S, Gimenez L (2021). Methods to study organogenesis in decapod crustacean larvae. I. larval rearing, preparation, and fixation. Helgol Mar Res 75:3. https://doi.org/10.1186/s10152-021-00548-x

Tziouveli V, Bastos-Gomez G, Bellwood O (2011). Functional morphology of mouthparts and digestive system during larval development of the cleaner shrimp Lysmata amboinensis (de Man, 1888). J Morphol 272:1080-91. https://doi.org/10.1002/jmor.10962

Vogt G (2019). Functional cytology of the hepatopancreas of decapod crustaceans. J Morphol 280:1405-44. https://doi.org/10.1002/jmor.21040

Vogt G (2008). Investigation of hatching and early postembryonic life of freshwater crayfish by in vitro culture, behavioral analysis, and light and electron microscopy. J Morphol 269:790-811. https://doi.org/10.1002/jmor.10622

Wägele J-W (1992). Isopoda. In: Harison FW, Humes AG, eds. Microscopic anatomy of invertebrates. Vol 9: Crustacea. New York: Wiley-Liss 529–617.

Walter A, Paul-Gilloteaux P, Plochberger B, Sefc L, Verkade P, Mannheim JG, Slezak P, Unterhuber A, Marchetti-Deschmann M, Ogris M, Bühler K, Fixler D, Geyer SH, Weninger WJ, Glösmann M, Handschuh S, Wanek T (2020). Correlated Multimodal Imaging in Life Sciences: Expanding the Biomedical Horizon. Front Phys 8:47. https://doi.org/10.3389/fphy.2020.00047

Wolff C (2009). The embryonic development of the malacostracan crustacean Porcellio scaber (Isopoda, Oniscidea). Dev Genes Evol 219:545–64. https://doi.org/10.1007/ s00427-010-0316-6

Žnidaršič N, Štrus J, Drobne D (2003). Ultrastructural alterations of the hepatopancreas in Porcellio scaber under stress. Environ Toxicol Phar 13:161-74 https://doi.org/10.1016/S1382-6689(02)00158-8

Žnidaršič N, Zdešar K, Štrus J (2005). Microscopic characterization of hepatopancreatic S cells with regard to their role in copper homeostasis of isopods. In: Čeh M, Dražič G, Fidler S, eds. 7th Multinational Congress on Microscopy, Portorož, Slovenia, 2005 June 26-30; Ljubljana: Jožef Stefan Institute 251-52.